

# Nanoscale

Accepted Manuscript



This is an *Accepted Manuscript*, which has been through the Royal Society of Chemistry peer review process and has been accepted for publication.

*Accepted Manuscripts* are published online shortly after acceptance, before technical editing, formatting and proof reading. Using this free service, authors can make their results available to the community, in citable form, before we publish the edited article. We will replace this *Accepted Manuscript* with the edited and formatted *Advance Article* as soon as it is available.

You can find more information about *Accepted Manuscripts* in the [Information for Authors](#).

Please note that technical editing may introduce minor changes to the text and/or graphics, which may alter content. The journal's standard [Terms & Conditions](#) and the [Ethical guidelines](#) still apply. In no event shall the Royal Society of Chemistry be held responsible for any errors or omissions in this *Accepted Manuscript* or any consequences arising from the use of any information it contains.

## ARTICLE

## Size-Dependent Tuning of Horseradish Peroxidase Bioreactivity by Gold Nanoparticles

Cite this: DOI: 10.1039/x0xx00000x

Haohao Wu,<sup>a,b,c</sup> Yi Liu,<sup>b</sup> Meng Li,<sup>b</sup> Yu Chong,<sup>b</sup> Mingyong Zeng,<sup>a</sup> Y. Martin. Lo<sup>c</sup> and Jun-Jie Yin<sup>\*b</sup>Received 00th January 2014,  
Accepted 00th January 2015

DOI: 10.1039/x0xx00000x

www.rsc.org/

Molecules with diverse biological functions, such as heme peroxidases, can be useful tools for identifying potential biological effects of gold nanoparticles (AuNPs) at the molecular level. Here, using UV-Vis, circular dichroism, dynamic light scattering, and electron spin resonance spectroscopy, we report tuning of horseradish peroxidase (HRP) bioactivity by reactant-free AuNPs with diameters of 5, 10, 15, 30 and 60 nm (Au-5nm, Au-10nm, Au-15nm, Au-30nm and Au-60nm). HRP conjugation to AuNPs was observed with only Au-5nm and Au-10nm prominently increasing the  $\alpha$ -helicity of the enzyme to extents inversely related to their size. Au-5nm inhibited both HRP peroxidase activity toward 3,3',5,5'-tetramethylbenzidine and HRP Compound I/II reactivity toward 5,5-dimethyl-1-pyrroline N-oxide. Au-5nm enhanced HRP peroxidase activity toward ascorbic acid and HRP Compound I/II reactivity toward redox-active residues in the HRP protein moiety. Further, Au-5nm also decreased the catalase- and oxidase-like activities of HRP. Au-10nm showed similar, but weaker, effects, while Au-15nm, Au-30nm and Au-60nm had no effect. Results suggest that AuNPs can size-dependently enhance or inhibit HRP bioreactivity toward substrates with different redox potentials via a mechanism involving extension of the HRP substrate access channel and decline in the redox potentials of HRP catalytic intermediates.

### Introduction

The worldwide enthusiasm for nanotechnology has raised concerns about the potential health and environmental impacts of nanomaterials. Specifically, gold nanoparticles (AuNPs) have a number of useful attributes (e.g. unique optical properties, high electron density, chemical and colloidal stability, facile synthesis, and ease of functionalization) that translate into applications such as electronics (e.g. printable inks and electronic chips), catalysis (e.g. CO oxidation and borohydride reductions), drug and gene delivery, photothermal and photodynamic therapy, bioimaging, and biosensing.<sup>1</sup> The biological effects of nanomaterials at the cellular, organismal and ecological levels are known to depend on the basic interactions between nanomaterials and molecular pathways. Previous studies have demonstrated the size-dependent cellular internalization, intracellular localization, cellular effects, tissue distribution, and histological toxicity of AuNPs,<sup>2</sup> but our understanding of the molecular mechanisms underlying these effects has not advanced at the same pace as research into industrial applications.<sup>3,4</sup>

One avenue for improving our understanding is to examine the effects of AuNPs on molecules with fundamental biological roles. Heme proteins contain covalently or noncovalently bound heme prosthetic groups (iron porphyrin complexes) that allow proteins to carry out essential functions such as electron transfer in cellular respiration, small molecule (e.g. O<sub>2</sub>, CO and

NO) binding in systemic respiration and cardiac signal transduction, and redox catalysis in peroxidases, catalases and oxidases. The diverse functions of heme proteins originate from the varied protein scaffolds and the versatile heme states, e.g. ferrous, ferric, Compound I (Fe<sup>4+</sup>=O), Compound II (Fe<sup>4+</sup>-OH) and Compound III (Fe<sup>3+</sup>-OOH).<sup>5</sup> Recent studies have revealed that conformations and heme electronic structures of heme proteins can be altered by interacting with nanomaterials.<sup>6-8</sup> Direct electron transfer between nanomaterials and surface-adsorbed heme proteins has been reported in electrochemical studies.<sup>8-10</sup> These studies suggest that exposure to exogenous nanomaterials could possibly lead to subtle but deleterious alterations in the bioreactivity of heme proteins.

Heme peroxidase, which is among the most important heme proteins, plays beneficial roles in diverse biological processes such as host defense, stress response, signal transduction, and thyroid hormone synthesis.<sup>11</sup> In this paper, horseradish peroxidase (HRP) is used as an exemplar heme peroxidase, due to its versatile catalytic activity and easy accessibility.<sup>12</sup> First we characterized HRP conjugation to reactant-free colloidal AuNPs, and then the effects of AuNPs on the peroxidase activity, Compound I/II reactivity, catalase-like activity, and oxidase-like activity of HRP were examined.

### Materials and methods

## Chemicals

Ascorbic acid (AA), hydrogen peroxide (H<sub>2</sub>O<sub>2</sub>), HRP (type VI, 250-330 U/mg, R/Z 2.5-4.0), 3,3',5,5'-tetramethylbenzidine (TMB), and nicotinamide adenine dinucleotide (NADH) were purchased from Sigma (St. Louis, MO). Concentrations of HRP were determined by using the extinction coefficient  $\epsilon = 102 \text{ mM}^{-1}\text{cm}^{-1}$  at 403 nm. AuNPs (>99.0% reactant free) with diameters of 5, 10, 15, 30 and 60 nm (Au-5nm, Au-10nm, Au-15nm, Au-30nm and Au-60nm) were supplied in 0.1 mM phosphate buffered saline (PBS) by CytoDiagnostics (Burlington, Canada), and their concentrations were quantified by using the optical densities (OD) at the surface plasmon resonance (SPR) wavelengths. According to the manufacturer, the stock solutions (OD = 1) of Au-5nm, Au-10nm, Au-15nm, Au-30nm, and Au-60nm contained  $5.5 \times 10^{13}$ ,  $6.0 \times 10^{12}$ ,  $1.6 \times 10^{12}$ ,  $1.8 \times 10^{11}$ , and  $2.0 \times 10^{10}$  particles per mL respectively, and their molar particle concentrations were calculated as 91.4, 10.0, 2.7, 0.3, and 0.03 nM respectively. Reactant-free AuNPs having different sizes with equal OD values were assumed to possess essentially equal effective surface areas. Transmission electron microscopy images of AuNPs are shown in Fig. S1†. 5,5-Dimethyl-1-pyrroline N-oxide (DMPO) and 1-hydroxy-3-carboxy-2,2,5,5-tetramethylpyrrolidine hydrochloride (CPH) were obtained from Enzo Life Sciences (Farmingdale, NY). 4-Hydroxy-2,2,6,6-tetramethylpiperidine-1-<sup>15</sup>N-oxyl (<sup>15</sup>N-PDT) was supplied by Cambridge Isotope Laboratories, Inc. (Andover, MA).

## Instrumental characterization of enzyme-nanoparticle conjugation

UV-Vis spectra were recorded in a 1 cm path length quartz cell at room temperature using a Varian Cary 300 spectrophotometer (Varian Inc., Palo Alto, CA). The reaction mixture was composed of 1.1  $\mu\text{M}$  HRP, 10 mM PBS (pH 7.2), and AuNPs (OD = 0 or 0.4). Approximately 2 min after mixing,<sup>13</sup> three spectra were recorded for each sample to obtain an average spectrum from which the background spectrum of the buffer was subtracted. The simulated spectra were obtained by adding the spectra of HRP and AuNPs.

Circular dichroism (CD) measurements were carried out in a 0.5 cm path length quartz cell at 25 °C on a Jasco J-810 Spectropolarimeter (Jasco, Tokyo, Japan) equipped with a Peltier temperature controller (Agilent Technologies, Palo Alto, CA). The reaction mixture was composed of 1.1  $\mu\text{M}$  HRP, 10 mM PBS (pH 7.2), and AuNPs (OD = 0 or 0.2). Approximately 2 min after mixing, three spectra were recorded for each sample to obtain an average spectrum. The background spectrum of the buffer with or without AuNPs was recorded and subtracted.

The hydrodynamic diameters of AuNPs (OD = 0.9) in 10 mM PBS (pH 7.2) with or without 1.1  $\mu\text{M}$  HRP were measured at 25 °C about 2 min after mixing using a Zetasizer Nano ZS (ZEN 3600) dynamic light scattering (DLS) system (Malvern Instruments, Worcestershire, UK) equipped with a He-Ne red (633 nm) laser. Analyses were performed using Zetasizer Nano ZS software (DTS version 5.10, Malvern Instruments, Worcestershire, UK). Disposable plastic cuvettes (10 mm path length) were used as sample containers. For each sample, three DLS measurements were conducted. An automatic measurement duration setting and a detection angle of 173° (i.e. backscatter) were used. All sizes reported here were based on intensity average. The intensity average particle size was obtained using a general purpose (GP) analysis algorithm.

## Peroxidase activity assays

Peroxidase activity using TMB as the H-donor was estimated from the change in absorbance for the reaction mixture at 370 nm ( $\Delta_{370 \text{ nm}}$ ) at room temperature.<sup>14</sup> The reaction mixture was composed of 0.2  $\mu\text{M}$  HRP, 200  $\mu\text{M}$  TMB, 10 mM PBS (pH 7.2), 12.5  $\mu\text{M}$  H<sub>2</sub>O<sub>2</sub>, and various concentrations of AuNPs. About 2 min after the mixing of HRP, PBS and AuNPs, TMB and H<sub>2</sub>O<sub>2</sub> were added, and the time dependence for  $\Delta_{370 \text{ nm}}$  was then immediately recorded in a 1 cm path length quartz cell on a Varian Cary 300 spectrophotometer. Within the initial 100 s,  $\Delta_{370 \text{ nm}}$  increased linearly with time. The initial oxidation rate of TMB was indicated by the initial slope of  $\Delta_{370 \text{ nm}}$ .

Peroxidase activity using AA as the H-donor was estimated from the initial oxidation rate of AA in 10 mM PBS (pH 7.2).<sup>15</sup> At this pH, AA exists mainly in the form of ascorbate monoanion which is interchangeably represented by AA throughout this work. The initial oxidation rates of AA were measured from the change in absorbance at 265 nm, where spectrum for AA shows a maximum absorption ( $\epsilon = 1.5 \times 10^4 \text{ M}^{-1}\text{cm}^{-1}$ ). The reaction mixture was composed of 0.2  $\mu\text{M}$  HRP, 100  $\mu\text{M}$  AA, 10 mM PBS (pH 7.2), 12.5  $\mu\text{M}$  H<sub>2</sub>O<sub>2</sub>, and selected concentrations of AuNPs. About 2 min after the mixing of HRP, PBS and AuNPs, AA and H<sub>2</sub>O<sub>2</sub> were added, and the kinetic experiments were conducted immediately thereafter in a 1 cm path length quartz cell at room temperature using a Varian Cary 300 spectrophotometer. Within the initial 100 s, the absorbance decreased linearly with time. The initial AA oxidation rate ( $V_0$ ) is taken as  $m/\epsilon$  (where  $m$  is the slope of the linear portion of the curve,  $\epsilon$  is the ascorbate absorption coefficient at 265 nm).

## Compound I/II reactivity assays

Measurements of the Compound I/II reactivity toward DMPO were carried out at room temperature using a Bruker EMX electron spin resonance (ESR) spectrometer (Billerica, MA). The reaction mixture was composed of 17  $\mu\text{M}$  HRP, 50 mM DMPO, 10 mM PBS (pH 7.2), 17  $\mu\text{M}$  H<sub>2</sub>O<sub>2</sub>, and selected concentrations of AuNPs. Immediately after the mixing of HRP, PBS and H<sub>2</sub>O<sub>2</sub>, DMPO and AuNPs were added. Data collection began 1 min after sample mixing, and the spectra were recorded using the following settings: 20 mW microwave power, 1 G field modulation, and 100 G scan range. The ESR spectrum obtained (Fig. 3A, inset) was assigned to 5,5-dimethyl-2-pyrroline-N-oxyl (DMPOX) from its hyperfine coupling constants ( $a^{\text{N}} = 7.1 \text{ G}$  and  $a^{\text{H}} = 4.2 \text{ G}$ ),<sup>16</sup> and the intensity of the second peak was used to quantify the amount of DMPOX formed in the reaction system.

The spontaneous decay of Compound I was monitored to determine the Compound I/II reactivity toward redox-active residues in the HRP protein moiety. The reaction mixture was composed of 5  $\mu\text{M}$  HRP, 10 mM PBS (pH 7.2), 5  $\mu\text{M}$  H<sub>2</sub>O<sub>2</sub>, and selected concentrations of AuNPs. Immediately after the mixing of HRP, PBS and H<sub>2</sub>O<sub>2</sub>, AuNPs were added. The time-dependent change in absorbance at 403 nm, where spectrum for ferric HRP, i.e. native HRP, shows a maximum absorption, was then immediately recorded in a 1 cm path length quartz cell at room temperature using a Varian Cary 300 spectrophotometer. The percentage of residual Compound I was calculated according to Erman and Yonetani (1975) with some modifications.<sup>17</sup> To eliminate interference from the absorption of AuNPs, we determined the difference in extinction coefficient at 403 nm of native HRP minus Compound I (Fig. S2†). Residual Compound I (%) =  $[A_0 - A(t)] / [\Delta\epsilon \times C] \times 100$ ,

where  $A_0$  is the absorbance of the native HRP control in the presence of corresponding concentrations of AuNPs,  $A(t)$  is the absorbance of the reaction mixture at 403 nm at a time point  $t$ ,  $\Delta\epsilon$  is the difference in extinction coefficient at 403 nm of native HRP minus Compound I ( $49.5 \text{ mM}^{-1}\text{cm}^{-1}$ ), and  $C$  is the initial concentration of HRP.

### Catalase activity assay

ESR spin label oximetry was used to determine the catalase activity of HRP and/or AuNPs. The reaction mixture contained 0.2 mM  $^{15}\text{N}$ -PDT, 10 mM PBS (pH 7.2), 5 mM  $\text{H}_2\text{O}_2$ , 4.5  $\mu\text{M}$  HRP and/or selected concentrations of AuNPs. Approximately 2 min after the mixing of HRP, PBS and AuNPs,  $\text{H}_2\text{O}_2$  and  $^{15}\text{N}$ -PDT were added. Data collection began 1 min after sample mixing, and the spectra were recorded on a Bruker EMX ESR spectrometer using the following settings: 1 mW microwave power, 0.05 G field modulation, and 2 G scan range. The production of  $\text{O}_2$  was estimated using the increase in peak to peak line width of the  $^{15}\text{N}$ -PDT lower field ESR line according to Liu et al. (2014) (Fig. S3†).<sup>18</sup>

### Oxidase activity assay

The oxidase activity of HRP in the presence of NADH was determined by ESR spectroscopy. The reaction mixture contained 7.5 mM NADH, 10 mM PBS (pH 7.2), 0.02 mM CPH, 1.1  $\mu\text{M}$  HRP, and selected concentrations of AuNPs. Approximately 2 min after the mixing of HRP, PBS and AuNPs, NADH and CPH were added. Data collection began 1 min after sample mixing, and the spectra were recorded on a Bruker EMX ESR spectrometer using the following settings: 20 mW microwave power, 1 G field modulation, and 100 G scan range. The oxidase activity was estimated from CPH oxidation which was indicated by the increase of intensity for the second peak of the CP• spectrum.

## Results and discussion

### Characterization of the enzyme-nanoparticle conjugation

Non-covalent conjugation of AuNPs to surrounding biomolecules can be achieved through electrostatic and hydrophobic interactions, providing the basis for electron and energy transfer between AuNPs and biomolecules. We characterized the conjugation of AuNPs to HRP at physiological pH using UV-Vis, CD and DLS spectroscopy.

The UV-Vis spectra of HRP, AuNPs, and their mixtures at pH 7.2 are shown in Fig. 1A and Fig. S4†; these figures also display the simulated spectra of the mixtures as calculated by combining the spectra of HRP and AuNPs. The presence of HRP resulted in 2, 4, 3, 2, and 2 nm reproducible redshifts of the SPR absorption peaks of Au-5nm, Au-10nm, Au-15nm, Au-30nm, and Au-60nm respectively, and no red-shift was observed from the simulated spectra. This indicates that the redshifts are due to the protein conjugation on the surface of AuNPs rather than the spectrum superposition.<sup>19</sup> The experimental SPR intensities of AuNPs in the presence of HRP were higher than those simulated, which indicates that HRP increased the local refractive index near the particle surface. This further confirms the conjugation of HRP to AuNPs. The presence of Au-5nm, Au-10nm, Au-15nm, Au-30nm, and Au-60nm changed the Soret band of HRP at 403 nm to 398, 401, 401, 401, and 402 nm, respectively, when evaluated both experimentally and through numerical simulations. Further, the

difference spectra of HRP obtained by the subtraction of the spectra of AuNPs from those of the mixture displayed no blue-shifts of the Soret band (Fig. S5†). Thus the blue-shifts of the Soret band were due to the spectrum superposition rather than to any enzyme-nanoparticle conjugation, suggesting that AuNPs did not change the non-planarity or the energy of the  $\pi$ - $\pi^*$  transition of the porphyrin ring in the HRP heme group.<sup>20,21</sup> The presence of AuNPs did increase the Soret intensities of HRP, *i.e.*, the probability of the  $\pi$ - $\pi^*$  transition of the porphyrin cycle in the heme group,<sup>20</sup> as compared to the simulated spectra, suggesting that AuNPs changed the symmetry of the HRP porphyrin ring.<sup>7</sup> In comparison to the simulated spectra, the presence of Au-5nm, Au-10nm, Au-15nm, Au-30nm, and Au-60nm decreased the absorption peak of HRP at 198 nm, *i.e.*, the probability of  $\pi$ - $\pi^*$  transition of the amide groups in the polypeptide backbone,<sup>22</sup> by  $7.9\pm 0.4\%$ ,  $4.5\pm 0.3\%$ ,  $2.7\pm 0.4\%$ ,  $1.1\pm 0.5\%$ , and  $1.4\pm 0.3\%$  respectively, which indicates that the interaction of AuNPs with the HRP polypeptide backbone is size-dependent.<sup>23</sup>

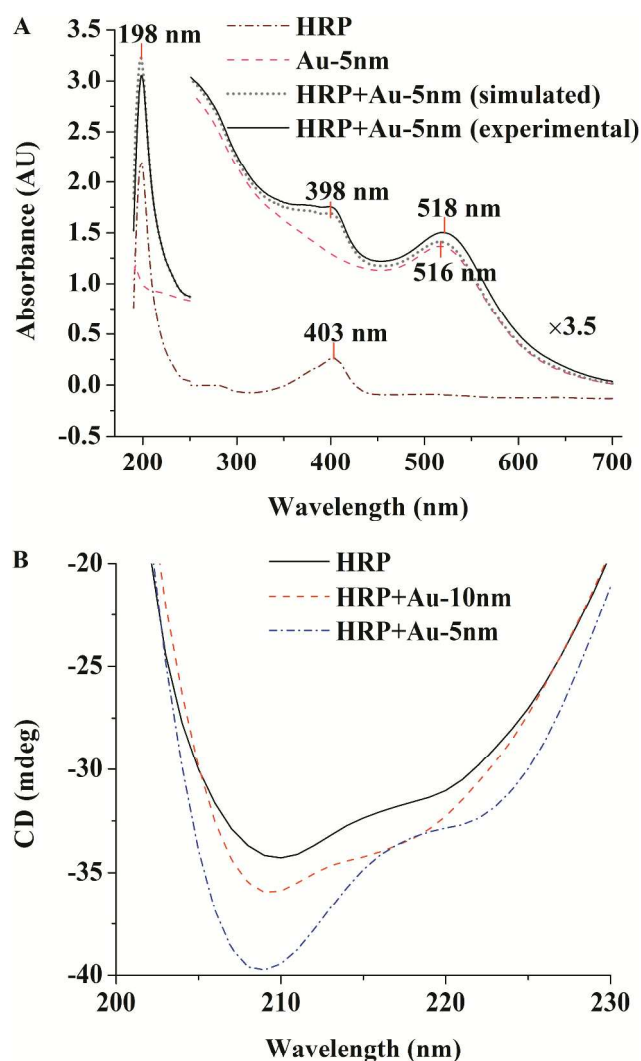
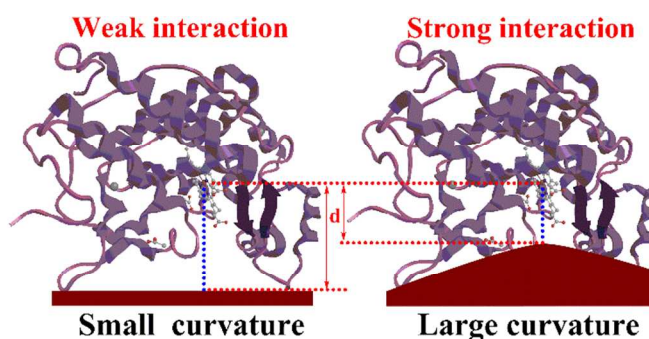


**Fig. 1.** Characterization of the enzyme-nanoparticle conjugation. (A) The UV-Vis spectra of HRP (1.1  $\mu\text{M}$ ), Au-5nm (OD = 0.4), and their mixture in 10 mM PBS (pH 7.2). The simulated spectrum was the result of adding the spectra of HRP and Au-5nm. The background spectrum of the buffer has been subtracted. (B) The far-UV CD spectra of HRP (1.1  $\mu\text{M}$ ) in the absence or presence of Au-5nm or Au-10nm (OD = 0.2) in 10 mM PBS (pH 7.2). The background spectrum of the buffer in the absence or presence of AuNPs has been subtracted.

Fig. 1B presents the far-UV CD spectra of HRP in the absence or presence of Au-5nm or Au-10nm at pH 7.2. The structure of HRP is largely  $\alpha$ -helical although there is also a small region of  $\beta$ -sheet.<sup>12</sup> A protein with abundant  $\alpha$ -helical secondary structures usually displays two negative peaks at around 208 nm and 222 nm. In the present study, HRP showed double negative peaks at around 208 nm and 222 nm, which is in accordance with previous reports.<sup>23</sup> The presence of Au-5nm increased the intensities of the two negative peaks of HRP, which indicates that the conjugation of Au-5nm to HRP can increase the  $\alpha$ -helicity of the enzyme. The presence of Au-10nm exhibited a similar effect to a lesser extent, while the presence of Au-15nm, Au-30nm, and Au-60nm did not show any effect on the far-UV CD spectra of HRP (data not shown).

DLS measurements revealed that HRP induced  $6.1 \pm 0.6$ ,  $6.8 \pm 0.7$ ,  $8.4 \pm 1.1$ ,  $7.3 \pm 0.7$ , and  $7.5 \pm 2.3$  nm diameter changes to Au-5nm, Au-10nm, Au-15nm, Au-30nm, and Au-60nm, respectively. HRP is a protein with a dimension of  $4.0 \times 6.8 \times 11.7$  nm<sup>3</sup> according to X-ray crystallography (Protein Data Bank ID code 1H5A), and was in much excess according to the molar concentrations of the enzyme (1.1  $\mu$ M) and the particles (less than 0.05  $\mu$ M) used here. The adsorption of HRP onto surfaces of AuNPs thus seemed to adopt the side-on orientation.<sup>24</sup>

Conformational changes of proteins induced by adsorption to surfaces have been found to depend on the surface topographic attributes, especially surface curvature at the



**Scheme 1.** Illustration of the HRP adsorption to surface with a small or large curvature.

nanoscale.<sup>25-27</sup> The surface curvature of spherical particles increases with decreasing core size. As shown in Scheme 1, a certain degree of curvature is required for an interaction of the surface with the inner cavity of HRP, which might explain the larger extent of interaction of smaller AuNPs with the amide groups in the HRP polypeptide backbone. The more interaction of Au-5nm and Au-10nm with the HRP polypeptide backbone might thus induce a more compact conformation (*i.e.* an increased  $\alpha$ -helicity) of the enzyme.

#### The peroxidase activity

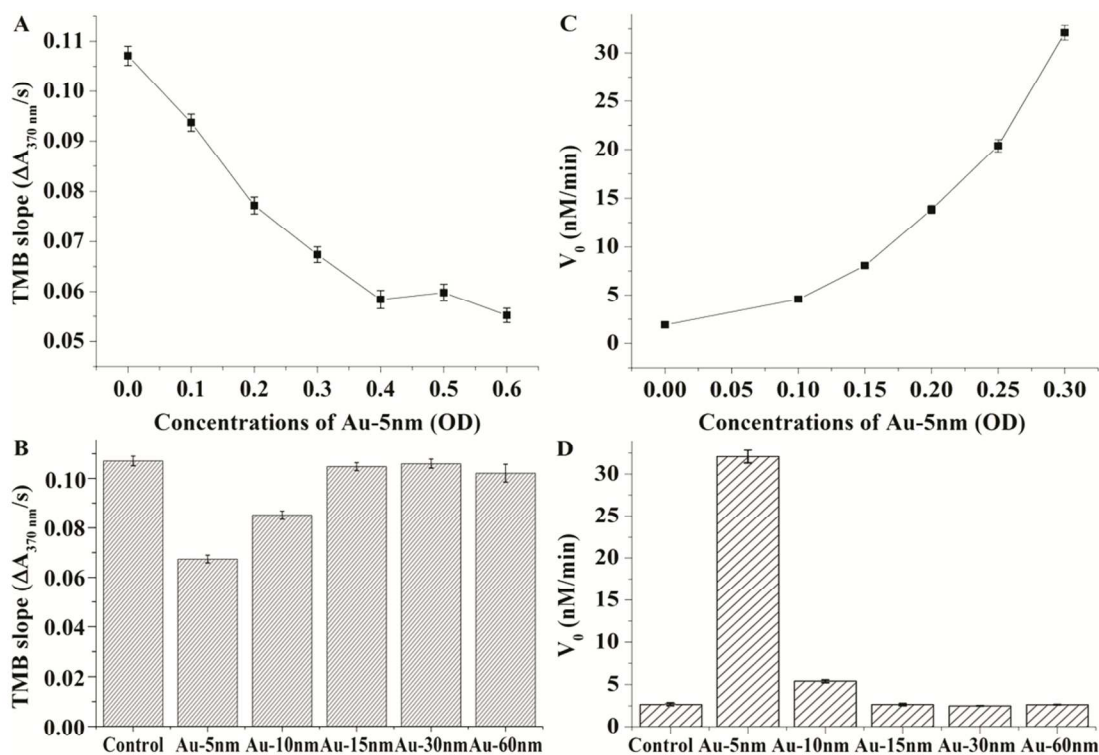


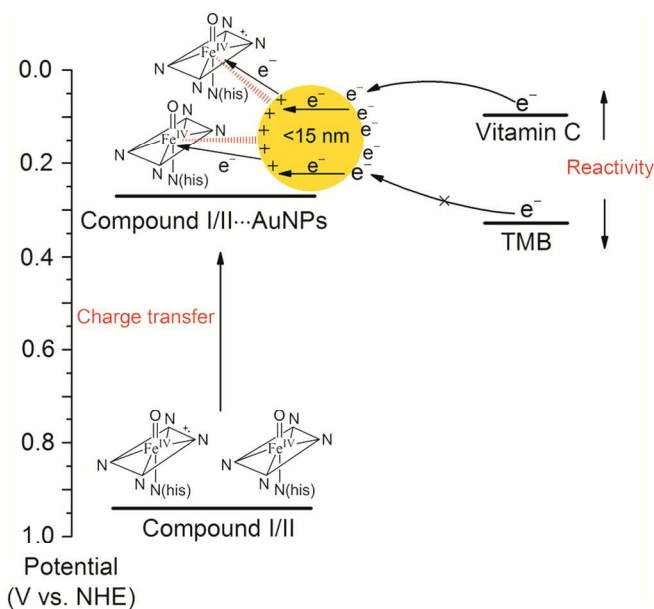
**Fig. 2.** Effects of (A, C) Au-5nm at different concentrations and (B, D) 0.3 OD of AuNPs with selected sizes on the oxidation rates of (A, B) TMB and (C, D) AA in the reaction mixtures consisted of 0.2  $\mu$ M HRP, 12.5  $\mu$ M H<sub>2</sub>O<sub>2</sub>, and 200  $\mu$ M TMB or 100  $\mu$ M AA in 10 mM PBS (pH 7.2).  $\Delta A_{370 \text{ nm}}$  represents the TMB oxidation products.

When the amount of TMB greatly exceeds that of  $H_2O_2$ , HRP will catalyze the formation of the charge-transfer complex of TMB and its two-electron (diimine) oxidation product.<sup>14</sup> This charge-transfer complex shows an absorption peak at 370 nm, so the initial slope of  $\Delta_{370\text{ nm}}$ , *i.e.*, the initial oxidation rate of TMB, represents the HRP peroxidase activity toward TMB. As shown in Fig. 2A, the peroxidase activity of HRP toward TMB decreased linearly as the concentration of Au-5nm increased from 0 to 0.4 OD ( $P < 0.025$ ). No further significant decline was observed when the concentration of Au-5nm exceeded 0.4 OD. Fig. 2B shows the size-dependent effects of AuNPs on the peroxidase activity of HRP toward TMB. Au-10nm displayed an inhibitory effect to a lesser extent than Au-5nm, while Au-15nm, Au-30nm, and Au-60nm had no significant effect.

The initial AA oxidation rate ( $V_0$ ) was used to indicate the HRP peroxidase activity toward AA. As shown in Fig. 2C, the peroxidase activity of HRP toward AA increased exponentially as the concentration of Au-5nm increased from 0 to 0.3 OD ( $P < 0.01$ ). Fig. 2D shows the size-dependent effects of AuNPs on the peroxidase activity of HRP toward AA. Au-10nm displayed an enhancing effect to a lesser extent than Au-5nm, while Au-15nm, Au-30nm, and Au-60nm showed no significant effect.

HRP catalyzes the oxidation of a variety of substrates by  $H_2O_2$  through its catalytic intermediates Compound I and Compound II, which have two and one oxidizing equivalents, respectively. Both HRP and AuNPs have been reported to possess the catalase-like activity.<sup>28,29</sup> The inhibitory effects of Au-5nm and Au-10nm on the peroxidase activity of HRP toward TMB may therefore be explained by the decreased Compound I/II reactivity toward TMB or the increased dismutation rate of  $H_2O_2$ . As will be presented later in Section 3.4, the catalase-like activity of the mixture of Au-5nm/Au-10nm and HRP was lower than that of HRP alone, so decreased Compound I/II reactivity of HRP toward TMB, rather than increased dismutation rate of  $H_2O_2$  in the reaction system, can be expected to explain the decreased HRP peroxidase activity toward TMB. The saturated inhibition of the HRP (200 nM) peroxidase activity toward TMB by 0.4 OD (36.6 nM) of Au-5nm indicates that full coverage of the particle surface of Au-5nm requires about 5.5 HRP molecules.

Previous experimental studies by our group have found that AuNPs do not display peroxidase-like activity under neutral and alkaline conditions,<sup>28</sup> therefore we expect that any increased peroxidase activity of HRP toward AA in the presence of AuNPs would be explained by the increased



**Scheme 2.** Illustration of tuning of HRP peroxidase activity by AuNPs.

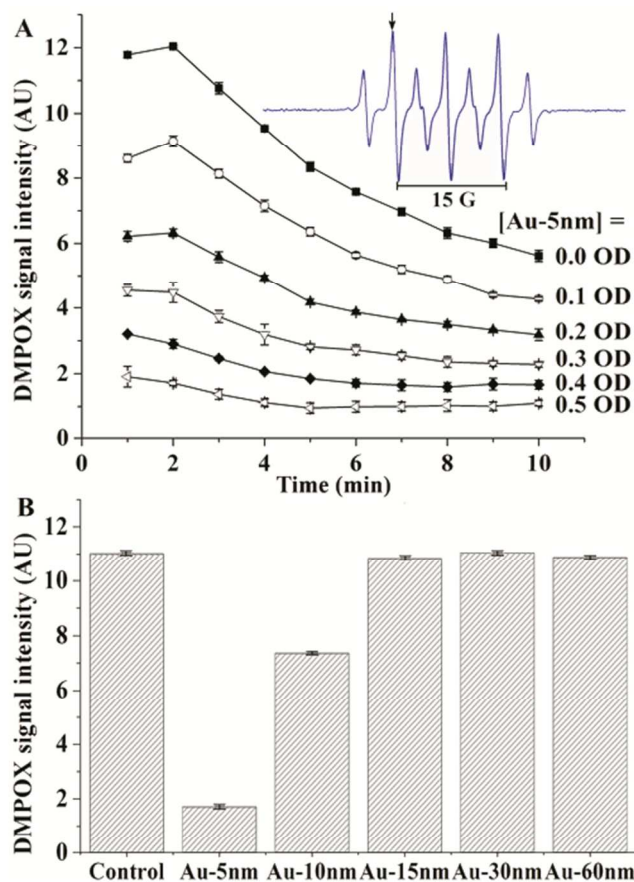
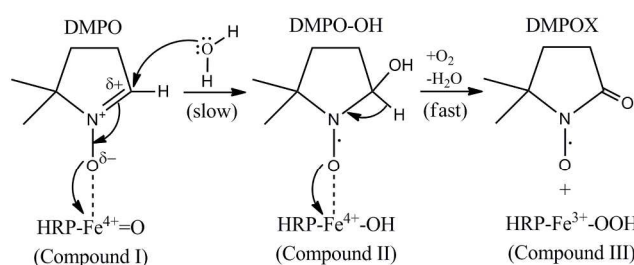


**Fig. 3.** Effects of (A) Au-5nm at different concentrations and (B) 0.5 OD of AuNPs with selected sizes on DMPOX production in the reaction mixture consisting of 17  $\mu\text{M}$  HRP, 50 mM DMPO, and 17  $\mu\text{M}$   $H_2O_2$  in 10 mM PBS (pH 7.2). DMPOX is the three-electron oxidation product of DMPO. The inset shows the typical ESR spectrum of DMPOX observed from the reaction mixture. The data in panel (B) are representative of results at 2 min of reaction time.

Compound I/II reactivity toward AA, rather than the peroxidase-like activity of AuNPs. Consequently, it is very intriguing that we observed divergent effects of Au-5nm and Au-10nm on the HRP Compound I/II reactivity toward TMB and AA. Considering the well-documented direct electron transfer between AuNPs and heme proteins,<sup>8-10</sup> charge transfer from HRP Compound I/II to AuNPs is possible, so electrons from the substrate could possibly be transferred to the active site of HRP via the conducting channels of AuNPs (Scheme 2).<sup>30</sup> This would mean that the HRP substrate access channel could be extended to surfaces of AuNPs.

On the other hand, the positive charge of Compound I/II could be dispersed over AuNPs due to the charge transfer, which would decrease the electron withdrawing nature of the group, *i.e.*, the redox potential of HRP Compound I/II.<sup>31</sup> The redox potentials of HRP Compound I and II have been reported as 0.92 and 0.94 V at pH 7.0, respectively.<sup>32</sup> AA is a well-known powerful reducing agent with a redox potential of about +60 mV at pH 7.0,<sup>33</sup> while TMB is a weak reductant with a redox potential of about +300 mV at pH 7.4.<sup>34</sup> The HRP Compound I/II redox potential thus seems to be lowered to a value within the range of +60 to +300 mV by Au-5nm and Au-10nm so that the divergent effects on the HRP peroxidase



**Scheme 3.** Schematic presentation of the reaction of HRP Compound I with DMPO.

activity toward TMB and AA can be explained. The extended substrate access channel should contribute to the enhancing effects of Au-5nm and Au-10nm on the HRP Compound I/II reactivity toward AA. As shown in Scheme 1, distance from particle surface to HRP iron center is dependent on surface curvature, which means that smaller AuNPs are closer to the HRP active site. Therefore, the inability of Au-15nm, Au-30nm and Au-60nm to tune HRP peroxidase activity is possibly due to longer charge-transfer distances.

### The Compound I/II reactivity

In order to validate our proposal about the extended substrate access channel and the lowered redox potential of HRP Compound I/II in the presence of AuNPs, Compound I was prepared by reaction of HRP with equal molar  $\text{H}_2\text{O}_2$ , followed by the examination of its reactivity toward DMPO and redox-active residues in the HRP protein moiety in the absence and

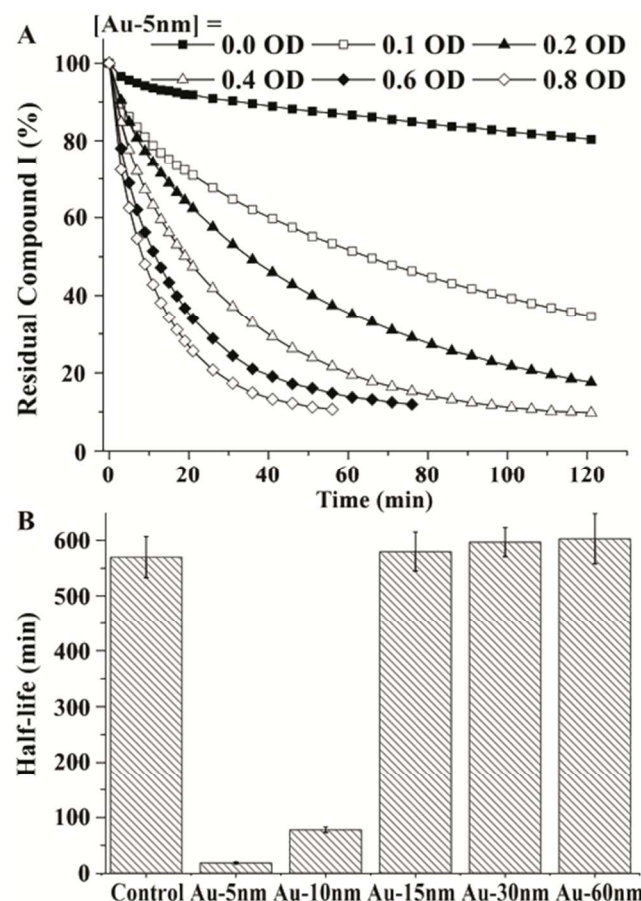


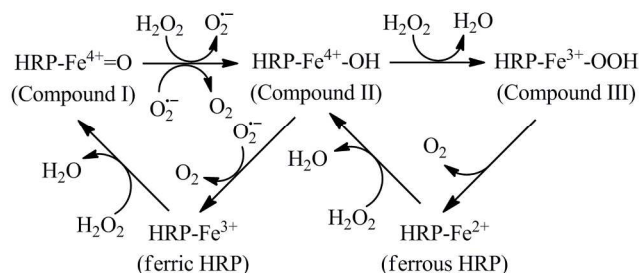
**Fig. 4.** Effects of (A) Au-5nm at different concentrations and (B) 0.4 OD of AuNPs with various sizes on the spontaneous decay of 5  $\mu\text{M}$  HRP Compound I in 10 mM PBS (pH 7.2). The residual percentage of Compound I was determined spectroscopically. Half-life is the amount of time required for the residual percentage of Compound I to fall to 50%.

presence of AuNPs.

DMPOX is the three-electron oxidation product of DMPO, and exhibits a six-line ESR signal (Fig. 3A, inset). As shown in Fig. 3A, DMPOX signal intensities increased rapidly to the maximum and then decreased slowly. The slow drop in DMPOX signal intensity can be explained by the dimerization of DMPOX and/or the reaction of DMPOX with excess DMPO.<sup>35</sup> Au-5nm markedly decreased the peak intensity of DMPOX in a dose-dependent manner (Fig. 3A). Au-10nm displayed an inhibitory effect to a lesser extent than Au-5nm, while Au-15nm, Au-30nm, and Au-60nm had no significant effect (Fig. 3B).

As shown in Scheme 3, an assumed reaction scheme for HRP Compound I oxidation of DMPO is proposed based on previously published studies.<sup>36-38</sup> Compound I  $\cdots$ DMPO is formed via electrostatic interaction, in a manner similar to the formation of  $\text{DMPO} \cdots \text{Fe}^{3+}/\text{Cu}^{2+}/\text{cytochrome c-Fe}^{4+}=\text{O}$  (Lewis acids), followed by the formation of Compound II  $\cdots$ DMPO-OH (2-hydroxy-5,5-dimethyl-1-pyrrolidinyloxy) via the Forrester-Hepburn mechanism, i.e. nucleophilic addition of a water molecule at the C-2 atom of DMPO and intramolecular electron transfer from DMPO to HRP Compound I, and the resultant complex readily reacts with dissolved oxygen to form Compound III and DMPOX. The Forrester-Hepburn reaction is the rate-determining step, and depends greatly on the electron withdrawing nature (i.e. redox potential) of the ionically bonded Lewis acid. Therefore, oxidation of DMPO was used in the present study to confirm a AuNPs-mediated decline in the redox potential of HRP compound I/II. The decreased peak intensities of DMPOX in the presence of Au-5nm and Au-10nm suggest the decreased oxidation rates of DMPO, i.e. the lowered redox potentials of HRP Compound I/II.

Compound I decays spontaneously upon its formation; we kinetically determined its residual percentage using a spectroscopic method. The spontaneous decay of HRP Compound I to the native enzyme via Compound II is a slow process (Fig. 4) due to the lack of available endogenous electron donors in the heme pocket.<sup>39</sup> Au-5nm dose-dependently accelerated this process (Fig. 4A). Au-10nm displayed a similar but weaker effect, while Au-15nm, Au-30nm, and Au-60nm displayed no significant effect (Fig. 4B). Tyrosine and tryptophan are mostly oxidized residues during spontaneous decay of peroxidases,<sup>40</sup> and their reduction potentials in proteins can be shifted to quite low values depending on sequences and conformations of the proteins.<sup>41,42</sup> It is thus not surprising that Compound I/II with a lowered reduction potential in the presence of Au-5nm or Au-10nm still obtained electrons from the HRP protein moiety. The accelerated spontaneous decay of HRP Compound I suggests long-range shuttling of electrons from endogenous donors to heme iron centers via the conducting channels of AuNPs, which further supports the view that adsorption of HRP onto Au-5nm



**Scheme 4.** Schematic presentation of the catalase-like activity of HRP.

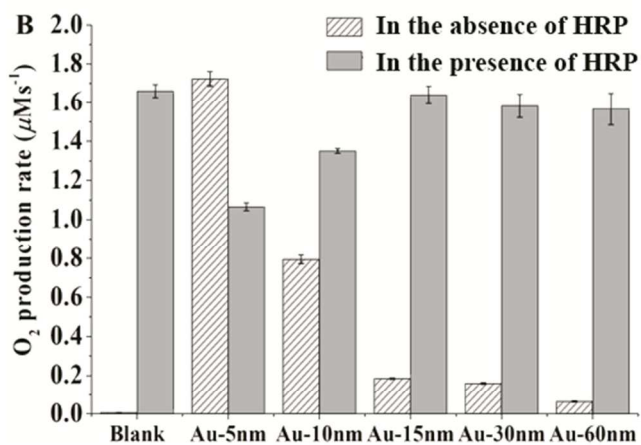
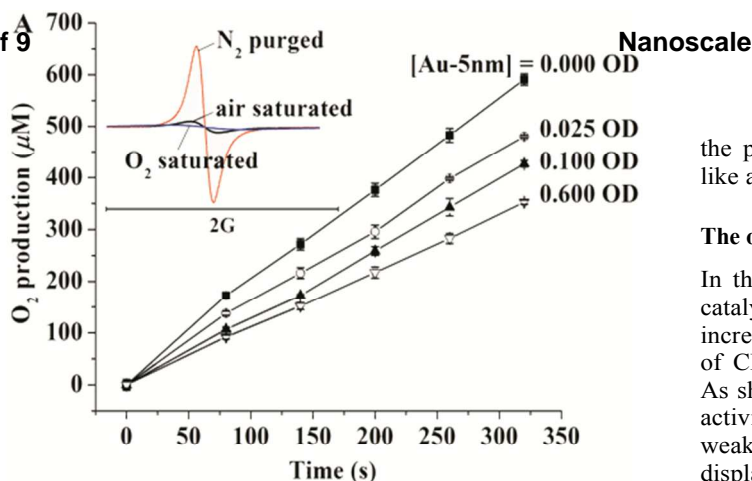


**Fig. 5.** Effects of (A) Au-5nm at different concentrations and (B) 0.6 OD of AuNPs with selected sizes on oxygen production in the reaction mixture consisting of 4.5  $\mu\text{M}$  HRP, 0.2 mM  $^{15}\text{N}$ -PDT, and 5 mM  $\text{H}_2\text{O}_2$  in 10 mM PBS (pH 7.2). Production of  $\text{O}_2$  was determined by monitoring the broadening of the  $^{15}\text{N}$ -PDT lower field ESR line. The inset in panel (A) is the ESR spectrum of  $^{15}\text{N}$ -PDT in air saturated,  $\text{O}_2$  saturated, and  $\text{N}_2$  purged solutions.

or Au-10nm can result in an extension of substrate access channel of the enzyme.

### The catalase-like activity

In the absence of suitable electron donors, HRP Compound I/II is able to oxidize  $\text{H}_2\text{O}_2$  into  $\text{O}_2$  via  $\text{O}_2^{\cdot-}$  (Scheme 4),<sup>43</sup> which is known as ‘‘catalase-like’’. In the present study, the production of  $\text{O}_2$  was determined by monitoring the broadening of the  $^{15}\text{N}$ -PDT lower field ESR line. Fig. 5A displays the dose-dependent inhibition of catalase-like activity of HRP by Au-5nm. Au-10nm showed a similar but weaker effect, while Au-15nm, Au-30nm, and Au-60nm displayed no significant effect (Fig. 5B). AuNPs alone also possessed the catalase-like activity depending on their size, but their catalase-like activity seemed to be inhibited by the surface-adsorbed HRP molecules based on the data of Au-5nm (Fig. 5B). As mentioned above, the redox potential of HRP Compound I/II could be lowered by the presence of Au-5nm and Au-10nm, while the one-electron redox potential of  $\text{H}_2\text{O}_2$  is as high as +0.89 at pH 7.<sup>44</sup> Therefore, Au-5nm and Au-10nm inhibited the catalase-like activity of HRP probably via decreasing the Compound I/II reactivity of the enzyme toward  $\text{H}_2\text{O}_2$ , and the larger sized particles had less effect because the active site of HRP is less affected by particles with a smaller curvature. The surface-adsorbed HRP molecules might reduce the access of  $\text{H}_2\text{O}_2$  to

the particle surface, thereby decreasing the intrinsic catalase-like activity of AuNPs.

### The oxidase-like activity

In the presence of NADH, HRP can act like an oxidase, i.e. catalyze the  $\text{O}_2$ -dependent oxidation of substrates. The intensity increasing of the three-line ESR signal of  $\text{CP}^\bullet$ , i.e. the oxidation of CPH, was used to evaluate the HRP oxidase-like activity. As shown in Fig. 6A, Au-5nm decreased the HRP oxidase-like activity dose-dependently. Au-10nm displayed a similar but weaker effect, while Au-15nm, Au-30nm, and Au-60nm displayed no significant effect (Fig. 6B). Pyridine nucleotide coenzymes activate oxidase cycles of HRP by reducing ferric HRP to ferrous HRP.<sup>45</sup> The one-electron redox potential of  $\text{NAD}^\bullet$  (nicotinamide adenine dinucleotide radical)/NADH at pH 7 is +282 mV,<sup>46</sup> while that for  $\text{Fe}^{3+}/\text{Fe}^{2+}$  couple in HRP is only a little higher value, +306 mV.<sup>47</sup> The one-electron reduction of ferric HRP by NADH is thus the rate limiting step in activation of oxidase cycles of the enzyme.<sup>48</sup> Au-5nm and Au-10nm decreased HRP oxidase-like activity probably via bringing down the redox potential of ferric HRP, which suggests the occurrence of charge transfer from ferric HRP to

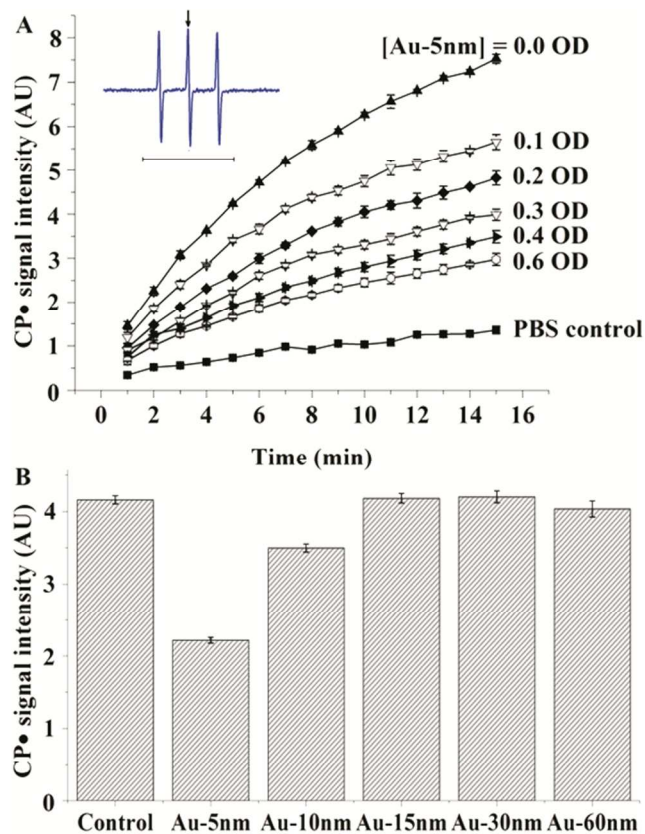


**Fig. 6.** Effects of (A) Au-5nm at different concentrations and (B) 0.3 OD of AuNPs with selected sizes on  $\text{CP}^\bullet$  nitroxide signal intensity in the reaction mixture consisting of 1.1  $\mu\text{M}$  HRP, 7.5 mM NADH and 20  $\mu\text{M}$  CPH in 10 mM PBS (pH 7.2). The inset in panel (A) is the typical ESR spectrum of  $\text{CP}^\bullet$  nitroxide resulted from the reaction mixture. The data in panel (B) are representative of results at 5 min of reaction time.

AuNPs.

## Conclusions

As shown by UV-Vis, CD, DLS, and ESR spectroscopy, we have demonstrated that AuNPs can size-dependently enhance or inhibit HRP bioreactivity toward substrates with different redox potentials via a mechanism involving extension of the HRP substrate access channel and decline in the redox potentials of HRP catalytic intermediates. Our results suggest that the divergent effects of AuNPs on the bioreactivity of heme proteins toward various substrates should be considered in biomedical applications under different circumstances.

## Acknowledgements

This article is not an official US Food and Drug Administration (FDA) guidance or policy statement. No official support or endorsement by the US FDA is intended or should be inferred. We acknowledge the support of the Maryland NanoCenter and its Nanoscale Imaging Spectroscopy and Properties (NISIP) Laboratory. This work was supported by a regulatory science grant under the FDA Nanotechnology CORES Program. H. Wu and M. Zeng appreciate the support from National Natural Science Foundation of China (No. 31371758), National Key Technology Research and Development Program of China (No. 2012BAD28B05), and China Scholarship Council (No. 201306330015). We thank Dr. Wayne G. Wamer (CFSA/FDA) for valuable suggestions and comments on this manuscript, and Dr. Lili Fox Vélez for her scientific editing support.

## Notes and references

<sup>a</sup> College of Food Science and Engineering, Ocean University of China, 5 Yushan Road, Qingdao, Shandong Province 266003, China.

<sup>b</sup> Division of Analytical Chemistry, Office of Regulatory Science, Center for Food Safety and Applied Nutrition, U.S. Food and Drug Administration, College Park, MD 20740, USA.

<sup>c</sup> Department of Nutrition and Food Science, University of Maryland, College Park, MD 20742, USA. E-mail: junjie.yin@fda.hhs.gov

† Electronic Supplementary Information (ESI) available. See DOI: 10.1039/b000000x/

- 1 L. Dykman and N. Khlebtsov, *Chem. Soc. Rev.*, 2012, **41**, 2256–2282.
- 2 N. Khlebtsov and L. Dykman, *Chem. Soc. Rev.*, 2011, **40**, 1647–1671.
- 3 Z. He, J. Liu and L. Du, *Nanoscale*, 2014, **6**, 9017–9024.
- 4 R. Coradeghini, S. Gioria, C. P. Garcia, P. Nativo, F. Franchini, D. Gilliland, J. Ponti and F. Rossi, *Toxicol. Lett.*, 2013, **217**, 205–216.
- 5 Y. W. Lin and J. Wang, *J. Inorg. Biochem.*, 2013, **129**, 162–171.
- 6 D. Sahoo, P. Bhattacharya, H. K. Patra, P. Mandal and S. Chakravorti, *J. Nanopart. Res.*, 2011, **13**, 6755–6760.
- 7 X. Jiang, J. Jiang, Y. Jin, E. Wang and S. Dong, *Biomacromolecules*, 2005, **6**, 46–53.
- 8 Q. Shao, P. Wu, P. Gu, X. Xu, H. Zhang and C. Cai, *J. Phys. Chem. B*, 2011, **115**, 8627–8637.
- 9 J.J. Feng, G. Zhao, J.J. Xu and H. Y. Chen, *Anal. Biochem.*, 2005, **342**, 280–286.

- 10 P. S. Jensen, Q. Chi, F. B. Grumsen, J. M. Abad, A. Horwell, D. J. Schiffrin, and J. J. Ulstrup, *Phys. Chem. C*, 2007, **111**, 6124–6132.
- 11 A. M. English and G. Tsapraillis, *Adv. Inorg. Chem.*, 1995, **43**, 79–125.
- 12 N. C. Veitch, *Phytochemistry*, 2004, **65**, 249–259.
- 13 Y. Ni, J. Li, Z. Huang, K. He, J. Zhuang and W. Yang, *J. Nanopart. Res.*, 2013, **15**, 1–10.
- 14 P. D. Josephy, T. Eling and R. P. Mason, *J. Biol. Chem.*, 1982, **257**, 3669–3675.
- 15 M. Scarpa, F. Vianello, L. Signor, L. Zennaro and A. Rigo, *Inorg. Chem.*, 1996, **35**, 5201–5206.
- 16 R. A. Floyd and L. M. Soong, *Biochem. Biophys. Res. Commun.*, 1977, **74**, 79–84.
- 17 J. E. Erman and T. Yonetani, *Biochim. Biophys. Acta.*, 1975, **393**, 350–357.
- 18 Y. Liu, H. Wu, M. Li, J.J. Yin and Z. Nie, *Nanoscale*, 2014, **6**, 11904–11910.
- 19 A. D. Phan, T. X. Hoang, T. H. Nghiem and L. M. Woods, *Appl. Phys. Lett.*, 2013, **103**, 163702.
- 20 J. A. Shelnett, C. J. Medforth, M. D. Berber, K. M. Barkigia and K. M. Smith, *J. Am. Chem. Soc.*, 1991, **113**, 4077–4087.
- 21 C. J. Medforth, M. O. Senge, K. M. Smith, L. D. Sparks and J. A. Shelnett, *J. Am. Chem. Soc.*, 1992, **114**, 9859–9869.
- 22 W. Al-Azzam, E. A. Pastrana, Y. Ferrer, Q. Huang, R. Schweitzer-Stenner and K. Griebenow, *Biophys. J.*, 2002, **83**, 3637–3651.
- 23 L. Wang, A. Lu, T. Lu, X. Ding and X. Huang, *Biochimie*, 2010, **92**, 41–50.
- 24 H. Jans, X. Liu, L. Austin, G. Maes and Q. Huo, *Anal. Chem.*, 2009, **81**, 9425–9432.
- 25 X. Sun, Z. Feng, L. Zhang, T. Hou and Y. Li, *PloS one*, 2014, **9**, e107696.
- 26 H. S. Mandal and H. B. Kraatz, *J. Am. Chem. Soc.*, 2007, **129**, 6356–6357.
- 27 A. C. Templeton, W. P. Wuelfing and R. W. Murray, *Acc. Chem. Res.*, 2000, **33**, 27–36.
- 28 W. He, Y. T. Zhou, W. G. Wamer, X. Hu, X. Wu, Z. Zheng, M. D. Boudreau and J. J. Yin, *Biomaterials*, 2013, **34**, 765–773.
- 29 A. N. Hiner, J. Hernández-Ruiz, G. A. Williams, M. B. Arnao, F. García-Cánovas and M. Acosta, *Arch. Biochem. Biophys.*, 2001, **392**, 295–302.
- 30 X. Yi, J. Huang-Xian and C. Hong-Yuan, *Anal. Biochem.*, 2000, **278**, 22–28.
- 31 A. R. Cross, J. Rae and J. T. Curnutte, *J. Biol. Chem.*, 1995, **270**, 17075–17077.
- 32 Y. Hayashi and I. Yamazaki, *J. Biol. Chem.*, 1979, **254**, 9101–9106.
- 33 H. Borsook and G. Keighley, *Proc. Natl. Acad. Sci. USA*, 1933, **19**, 875–878.
- 34 S. A. Trashin, T. Cucu, B. Devreese, A. Adriaens and B. De Meulenaer, *Anal. Chim. Acta.*, 2011, **708**, 116–122.
- 35 A. Nakajima, Y. Ueda, N. Endoh, K. Tajima and K. Makino, *Can. J. Chem.*, 2005, **83**, 1178–1184.
- 36 K. Rangelova and R. P. Mason, *Magn. Reson. Chem.*, 2011, **49**, 152–158.
- 37 A. Lawrence, C. M. Jones, P. Wardman and M. J. Burkitt, *J. Biol. Chem.*, 2003, **278**, 29410–29419.

## Journal Name

- 38 K. Makino, A. Hagi, H. Ide, A. Murakami and M. Nishi, *Can. J. Chem.*, 1992, **70**, 2818–2827.
- 39 V. P. Miller, D. B. Goodin, A. E. Friedman, C. Hartmann and P. R. Ortiz de Montellano, *J. Biol. Chem.*, 1995, **270**, 18413–18419.
- 40 A. F. Coulson and T. Yonetani, *Biochem. Biophys. Res. Commun.*, 1972, **49**, 391–398.
- 41 S. Navaratnam and B. J. Parsons, *J. Chem. Soc., Faraday Trans.*, 1998, **94**, 2577–2581.
- 42 J. Bergès, P. de Oliveira, I. Fourré and C. Houée-Levin, *J. Phys. Chem. B*, 2012, **116**, 9352–9362.
- 43 J. Vlasits, C. Jakopitsch, M. Bernroitner, M. Zamocky, P. G. Furtmüller and C. Obinger, *Arch. Biochem. Biophys.*, 2010, **500**, 74–81.
- 44 P. M. Wood, *Biochem. J.*, 1988, **253**, 287–289.
- 45 E. S. Kirkor and A. Scheeline, *Eur. J. Biochem.*, 2000, **267**, 5014–22.
- 46 R. F. Anderson, *Biochim. Biophys. Acta.*, 1980, **590**, 277–281.
- 47 G. Battistuzzi, M. Borsari, A. Ranieri and M. Sola, *J. Am. Chem. Soc.*, 2002, **124**, 26–27.
- 48 M. S. Afanasyeva, M. B. Taraban, P. A. Purtov, T. V. Leshina and C. B. Grissom, *J. Am. Chem. Soc.*, 2006, **128**, 8651–8658.